European Journal of Cancer 101 (2018) 165–180

Available online at www.sciencedirect.com

ScienceDirect

journal homepage: www.ejcancer.com

Original Research

Influence of eukaryotic translation initiation factor 6 on non–small cell lung cancer development and progression

Nadine Gantenbein [a,b], Eva Bernhart [c], Ines Anders [a], Nicole Golob-Schwarzl [a,b], Stefanie Krassnig [a], Christina Wodlej [a,b], Luka Brcic [a], Joerg Lindenmann [d], Nicole Fink-Neuboeck [d], Franz Gollowitsch [a], Elvira Stacher-Priehse [a], Martin Asslaber [a], Margit Gogg-Kamerer [a], Jana Rolff [e], Jens Hoffmann [e], Alessandra Silvestri [f], Christian Regenbrecht [f], Christoph Reinhard [g], Anna-Maria Pehserl [h], Martin Pichler [h], Olga Sokolova [i], Michael Naumann [i], Valentin Mitterer [j], Brigitte Pertschy [j], Helmut Bergler [j], Helmut Popper [a], Wolfgang Sattler [c], Johannes Haybaeck [a,b,k,*]

[a] *Diagnostic and Research Institute of Pathology, Medical University of Graz, Neue Stiftingtalstrasse 6, 8010 Graz, Austria*
[b] *Center for Biomarker Research in Medicine, Stiftingtalstrasse 5, 8010 Graz, Austria*
[c] *Gottfried Schatz Research Center for Cell Signaling, Metabolism and Aging, Molecular Biology and Biochemistry, Medical University of Graz, Neue Stiftingtalstrasse 6, 8010 Graz, Austria*
[d] *Division of Thoracic and Hyperbaric Surgery, Medical University of Graz, Auenbruggerplatz 29, 8036 Graz, Austria*
[e] *Experimental Pharmacology & Oncology Berlin GmbH-Berlin-Buch, Robert-Rössle-Str. 10, 13125 Berlin-Buch, Germany*
[f] *Cpo - Cellular Phenomics & Oncology Berlin-Buch GmbH, Robert-Rössle-Str. 10, 13125 Berlin-Buch, Germany*
[g] *Eli Lilly & Company, Lilly Corporate Center, 46285 Indiana, Indianapolis, USA*
[h] *Division of Oncology, Medical University of Graz, Auenbruggerplatz 15, 8036 Graz, Austria*
[i] *Institute of Experimental Internal Medicine, Otto-von-Guericke-University Magdeburg, Leipziger Str. 44, 39120 Magdeburg, Germany*
[j] *Institute of Molecular Biosciences, Karl-Franzens-University of Graz, Humboldtstraße 50, 8010 Graz, Austria*
[k] *Department of Pathology, Medical Faculty, Otto-von-Guericke-University Magdeburg, Leipziger Str. 44, 39120 Magdeburg, Germany*

Received 3 April 2018; received in revised form 22 June 2018; accepted 2 July 2018
Available online 1 August 2018

* *Corresponding author*: Department of Pathology, Otto-von-Guericke-University Magdeburg, Leipziger Straße 44, D-39120 Magdeburg, Germany. Fax: +49 391 67 15818.
E-mail address: johannes.haybaeck@med.ovgu.de (J. Haybaeck).

https://doi.org/10.1016/j.ejca.2018.07.001

KEYWORDS
Non–small cell lung cancer;
Adenocarcinoma;
Squamous cell carcinoma;
Eukaryotic translation initiation factor 6

Abstract Non–small cell lung cancer (NSCLC) is the leading cause of cancer-related death worldwide. Dysregulation of protein synthesis plays a major role in carcinogenesis, a process regulated at multiple levels, including translation of mRNA into proteins. Ribosome assembly requires correct association of ribosome subunits, which is ensured by eukaryotic translation initiation factors (eIFs). eIFs have become targets in cancer therapy studies, and promising data on eIF6 in various cancer entities have been reported. Therefore, we hypothesised that eIF6 represents a crossroad for pulmonary carcinogenesis. High levels of *eIF6* are associated with shorter patient overall survival in adenocarcinoma (ADC), but not in squamous cell carcinoma (SQC) of the lung. We demonstrate significantly higher protein expression of eIF6 in ADC and SQC than in healthy lung tissue based on immunohistochemical data from tissue microarrays (TMAs) and on fresh frozen lung tissue. Depletion of eIF6 in ADC and SQC lung cancer cell lines inhibited cell proliferation and induced apoptosis. Knockdown of *eIF6* led to pre-rRNA processing and ribosomal 60S maturation defects. Our data indicate that eIF6 is upregulated in NSCLC, suggesting an important contribution of eIF6 to the development and progression of NSCLC and a potential for new treatment strategies against NSCLC.

1. Introduction

Non–small cell lung cancer (NSCLC), accounting for more than 85% of newly diagnosed lung cancer, is the leading cause of cancer-related death worldwide [1,2]. Despite a large arsenal of treatment options, the future perspective for patients suffering from NSCLC is dismal, with a combined 5-year overall survival (OS) rate of ~15–18% [1,2].

This study investigates the role of eukaryotic translation initiation factor 6 (eIF6) in the two major subtypes of NSCLC, adenocarcinoma (ADC) with ~50% and squamous cell carcinoma (SQC) with ~40% occurrence [3,4]. ADCs occur primarily in the distal airways, whereas SQCs arise mainly in the proximal airways [3], indicating that the two entities differ morphologically and on the molecular level.

One of the major activities of a eukaryotic cell is ribosomal biosynthesis to ensure continuous protein translation. Thus, dysregulation of translation initiation has received considerable attention, and a number of studies revealed aberrant eukaryotic translation initiation factors (eIFs) expression in various cancer entities [5–13].

eIFs facilitate the formation of a translation-competent 80S ribosome, a rate-limiting step during carcinogenesis [14,15]. Translation initiation can be divided briefly into four steps: (1) formation of 43S pre-initiation complex by recruiting the ternary complex eIF2-GTP-tRNAi(met) to the small 40S ribosomal subunit, (2) assembly of the 48S initiation complex by 5′ cap recognition by eIF4F joining the 43S complex, (3) scanning of the mRNA starting from the 5′UTR region to the start codon and (4) formation of the mature 80S ribosome by joining the 60S subunit, which is accomplished by eIF5B and eIF6 [15,16]. The mammalian ribosome consists of a 60S (large) and a 40S (small) subunit. Its biogenesis starts in the nucleus where the precursor ribosomal RNAs (rRNA) 5S and 35S as well as ribosomal proteins and assembly factors (including eIF6) bind to either the pre-40S or pre-60S ribosomal subunit [17,18]. During the assembly process, the two subunits are transported into the cytoplasm, where eIF6 dissociates to facilitate binding of the 40S and 60S subunits [19,20]. The 40S subunit contains the 18S rRNA, whereas the 60S subunit comprises three rRNAs, 25S, 5.8S and 5S [17,21,22].

Recent studies suggest that eIF6, a 27-kDa protein, has a dual function [9,19]. It was first described as an anti-association factor that prevents assembly of the 40S and 60S ribosomal subunit [23,24]. On the other hand, eIF6 is necessary for ribosome biogenesis in the nucleus [25]. Previous studies report that eIF6 is an important factor in tumorigenesis, cell cycle progression and invasiveness of cancer cells [19,26,27]. In addition, the important cellular role of eIF6 was emphasised by a study in which mice with a total depletion of *eIF6* had a lethal phenotype [28]. Dysregulation of eIF6 was shown in various cancer entities, such as colorectal carcinoma (CRC) [13], malignant pleural mesothelioma (MPM) [9] and breast cancer [29]. In CRC and MPM, eIF6 was overexpressed compared to non-neoplastic tissue, suggesting a key contribution to carcinogenesis and highlighting eIF6 as a potential new biomarker [9,13]. In this study, we correlated eIF6 expression with patients' survival in pulmonary ADC and SQC and investigated how eIF6 expression affects tumorigenic properties of representative cell lines of these two NSCLC entities.

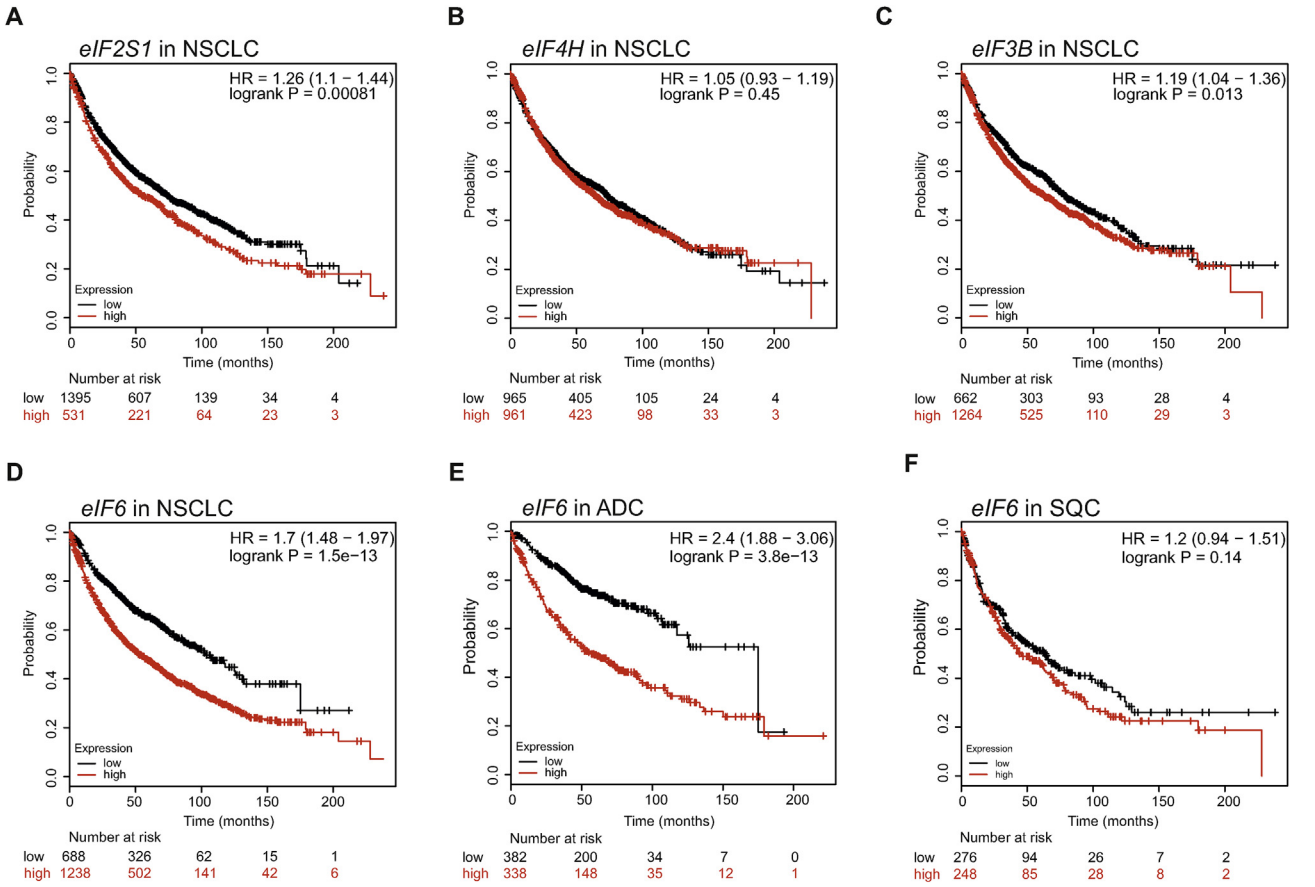

Fig. 1. *eIF6* expression is enhanced in ADC patients and associated with shorter OS. Kaplan–Meier plots comparing OS in NSCLC, ADC and SQC patients with different expression levels of eukaryotic translation initiation factors are shown. High expression is highlighted in red and low expression in black. eIF expression was analyzed in Affymetrix data set comprised of 1926 NSCLC patients. **(A)** Significant worse OS is found for patients with high *eIF2S1* ($p = 0.00081$), with a median hazard ratio (HR) of 1.26 (1.1–1.44), than for those with low *eIF2S1* expression. **(B)** *eIF4H* shows no significant impact in NSCLC on OS ($p = 0.45$) with a median HR of 1.05 (0.93–1.19) compared to low *eIF4H* expression. **(C)** High expression of *eIF3B* affects NSCLC OS ($p = 0.013$) with a median HR of 1.19 (1.04–1.36) compared to low *eIF4H* expression. **(D)** High expression levels of *eIF6* significantly correlate with shorter OS ($p = 1.5e-13$), with a median HR of 1.7 (1.48–1.97), than low *eIF6* expression. **(E)** Significantly shorter survival is observed for ADC ($n = 720$) patients with high *eIF6* expression ($p = 3.8e-13$) with median HR of 2.4 (1.88–3.06). **(F)** Patients with squamous cell carcinoma ($n = 524$) show no correlation between *eIF6* expression level ($p = 0.14$) and survival, and the median HR is 1.2 (0.98–1.51). ADC, adenocarcinoma; NSCLC, non–small cell lung cancer; SQC, squamous cell carcinoma; OS, overall survival.

2. Material and methods (see extended version in Appendix)

2.1. Ethics statement

The Ethics Committee of the Medical University of Graz, Austria, approved the collection and use of human lung specimens, according to the ethical guidelines of the 1975 Declaration of Helsinki (EK 27-240 ex 14/15). All samples and medical data used in this study were irreversibly anonymised.

2.2. Statistical analysis

For all statistical analyses and graph generation, GraphPad PRISM 5.0 edition software (GraphPad software Inc., La Jolla, CA, USA) was used. Except for tissue microarray (TMA) data, all data were analysed by the statistical software program SPSS (SPSS, Inc. Chicago, IL). All presented data were analysed by descriptive statistics and displayed as means ± standard error of means (SEM). Statistical tests according to each data set are mentioned in the figure legends. Each data set was analysed for Gaussian distribution. Normally distributed data were analysed by student t-test or one-way analysis of variance. Mann–Whitney U or Kruskal–Wallis test were used when data were not normally distributed. For all analyses, the alpha was set to 0.05.

2.3. Data availability

Original data are stored at the 'Mendeley Data' and available in [https://doi.org/10.17632/7r34pvvdvc.1].

3. Results

3.1. eIF6 expression is enhanced in ADC patients with shorter OS

To investigate the significance of eukaryotic translation initiation factors in OS, we explored two large independent cohorts of NSCLC patients. The screening cohort (Affymetrix data set, cohort 1) comprised expression data of 1,926 NSCLC patients with a follow-up time up to 15 years. High expression levels of *eIF2alpha* (eIF2S1, p = 8.1e − 4) and *eIF3B* (p = 1.3e − 2) were negatively associated with patient OS, whereas *eIF4H* expression analysis showed no significant impact on OS (Fig. 1A–C). Higher expression of *eIF6* in NSCLC showed significantly shorter OS compared with low levels of *eIF6* (hazard ratio [HR] = 1.7, 95% confidence interval = 1.48–1.97, p = 1.5e − 13) (Fig. 1D). Therefore, we refined our analysis to investigate *eIF6* expression and its association with survival in the two main subtypes of NSCLC, ADC and SQC. *eIF6* expression significantly correlated with OS in ADC patients (p = 3.8e − 13) with a HR of 2.4 (Fig. 1E), whereas there was no apparent correlation in SQC patients (Fig. 1F). Using a second independent validation cohort (The Cancer Genome Atlas [TCGA] data set, cohort 2), we could confirm these findings for both the NSCLC subtypes (Fig. S1A and B).

3.2. eIF6 is overexpressed in NSCLC patients

To further support the clinical relevance of our results. We studied eIF6 expression in ADC and SQC by immunohistochemistry (IHC) on TMA sections (Table 1). In ADC, 306 patient samples were analysed, and 152 non-neoplastic lung tissues (NNT) served as controls. eIF6 staining was mainly observed in the cytoplasm, and the tissue intensity score was significantly higher ($p < 0.0001$) in ADC tissue than in NNT (Fig. 2A). Analysis of staining intensity in ADC G1-G3 tumours revealed significant differences in eIF6 expression within these groups (p = 0.0400) in which staining increased significantly with higher grade for G1 versus G2 (p = 0.0140) and G1 versus G3 (p = 0.0470). When comparing G2 versus G3, no significant changes were observed (Fig. 2B). For SQC, 61 samples were stained for eIF6, which was also mainly located in the cytoplasm (Fig. 2C). Although eIF6 intensity was significantly higher in tumour samples than in 31 NNT samples ($p < 0.0001$), no significant differences were observed among the different grades in SQC (Fig. 2D).

To examine if eIF6 protein levels were also upregulated in freshly frozen lung tumour tissue compared with NNT, protein lysates of 14 ADC and 14 SQC tissue samples and the respective adjacent NNT were analysed, which revealed overexpression of eIF6 in most of the ADC and SQC tumours when compared with NNT (Fig. 2E–G). Within this patient subset, we analysed *eIF6* mRNA expression by quantitative real time PCR (qRT-PCR) and observed a significant upregulation of *eIF6* in ADC (p = 0.0080) and SQC (p = 0.0168) as compared with NNT (Fig. 2H). Clinicopathological characteristics see Table 2.

Table 1
Clinicopathological characteristics of patients assessed by TMA tissue specimens.

Adenocarcinoma	n = 306	%
Gender		
Female	120	39.2
Male	186	60.7
Grade		
G1	67	21.8
G2	124	40.5
G3	114	37.3
Tissue intensity score		
0	26	8.5
1	24	78.4
2	182	59.5
3	74	24.1
Non-neoplastic tissue	n = 152	%
Gender		
Female	67	44.1
Male	85	55.9
Tissue intensity score		
0	152	100.0
1	0	00.0
2	0	00.0
3	0	00.0
Squamous cell carcinoma	n = 62	%
Gender		
Female	10	16.1
Male	52	83.9
Grade		
G1	3	4.8
G2	37	59.7
G3	22	35.5
Tissue intensity score		
0	7	11.3
1	4	6.4
2	35	56.5
3	16	25.8
Smoking status		
Smoker	13	20.9
Non-smoker	2	3.2
Unknown status	47	75.8
Non-neoplastic tissue	n = 31	%
Gender		
Female	6	19.4
Male	25	80.6
Tissue intensity score		
0	31	100.0
1	0	00.0
2	0	00.0
3	0	00.0

3.3. Knockdown of eIF6 reduces proliferation in A549 and H520 cells

To evaluate the consequences of reduced eIF6 levels on cell proliferation, A549 (representing ADC) and H520

(representing SQC) cell lines were transfected with eIF6-targeting siRNA. To ensure comparable transfection efficacy, A549 and H520 cell lines were transfected with Alexa-488–labelled non-targeting siRNA. Fluorescence intensity was analysed by flow cytometry at 6 and 24 h after transfection. In both the cell lines, ≥90% of cells were Alexa-488 positive, indicating comparable transfection efficacy (Fig. S2A).

Knockdown efficacy of eIF6 was evaluated by Western blot (WB) analysis 3 and 5 days after transfection. eIF6 knockdown was efficient (approx. 80% at both time points analysed) in of if A549 cells regardless of the siRNA constructs were used individually or in combination (Fig. 3A and B). In H520 cells, silencing efficacy was lower (Fig. 3D). In this cell model, single siRNA constructs and the siRNA pool reduced eIF6 levels between 40 and 60% (Fig. 3E).

Analysis of *eIF6* mRNA levels in A549 3 d after silencing revealed a significant reduction by 80–90% after 3 d and by 50% after 5 d (Fig. 3C) compared with non-targeting scrambled siRNA (siScr). In contrast, mRNA levels in H520 cells were reduced by approximately 50% compared with siScr control cells 3 d after transfection, whereas no significant *eIF6* mRNA reduction was observed after 5 d (Fig. 3F).

The effect of eIF6 reduction on A549 and H520 proliferation was analysed by flow cytometrical cell counting. In A549 cells, transfection of eIF6 siRNA, either individually or in combination, significantly reduced cell numbers up to ~80% compared with untreated cells (Fig. 3G, *left panel*). Mock transfection and transfection with non-targeting siRNA inhibited proliferation up to 20%.

Similarly, mock and siScr transfection affected proliferation in H520 cells (Fig. 3G, *right panel*). A significant decrease in proliferation in response to eIF6 silencing was observed on day 5 after transfection, with a reduction of 30–50%, for all constructs compared to siScr.

In addition, colony formation of A549 and H520 cells was investigated after eIF6 knockdown (Fig. 3H). Compared to control cells, both the transfected cell lines developed evidently fewer colonies after 4 weeks of cultivation.

3.4. Reduced eIF6 levels trigger apoptosis

To study whether reduced cell proliferation due to eIF6 silencing is accompanied by apoptosis, annexin V-FITC (A)/propidium iodide staining was performed in A549 and H520 cells (Fig. 4A–D). For flow cytometric analysis (FACS), cells were either transfected with single siRNA constructs or in combination, and untreated, mock and siScr transfected cells were used as controls. Representative scatter blots of FACS analyses of A549 cells on day 5 after silencing demonstrated a significant increase in late apoptotic cells from 6% (siScr) to 27% (Fig. 4A; gated in the upper right quadrant) in response to eIF6 silencing (Fig. 4A). In H520, eIF6 silencing did not affect the apoptotic cell populations (early and late; Fig. 4B).

On day 3 after transfection, A549 viability was significantly reduced as compared to cells transfected with non-targeting siRNA. eIF6 knockdown revealed no significant effects on day 3, whereas the fraction of early and late apoptotic cells significantly increased at day 5 with both siRNA constructs (Fig. 4C, Table S4). In contrast, in H520 cells, eIF6 depletion did not induce apoptosis (Fig. 4D).

To define the activation of apoptotic pathways, cleavage of Caspase 3 (Casp 3) and PARP was assessed by WB analyses. In A549 both, PARP and Casp 3 cleavage was observed on day 3 and day 5 after silencing independently of whether individual or pooled siRNA constructs were used (Fig. 4E, G). In H520 cells, weak Casp 3 processing was observed on day 5 in response to eIF6 knockdown, whereas PARP cleavage was unaffected by eIF6 silencing (Fig. 4F, H).

To test whether eIF6 silencing induces senescence in these cell lines, senescence-associated β-galactosidase staining (day 4 after transfection) was performed. Indeed, β-galactosidase staining was observed after transfection in A549 (Fig. S3A) but not in H520 cells (Fig. S3A). To further confirm these findings, WB analyses of transfected cells were performed using an antibody against p21, a protein that inhibits CDK-1 and serves as an indicator for senescence. In A549, an increase in p21 immunoreactivity on day 5 was observed for eIF6-depleted cells compared with control cells (Fig. S3C). In H520 cells, p21 levels were unaffected by eIF6 silencing (Fig. S3D).

3.5. rRNA processing in pre-60S subunits is disturbed by knockdown of eIF6

Owing to the role of eIF6 in pre-60S subunit maturation, we investigated the impact of reduced eIF6 levels on ribosome biogenesis by ribosomal profiling on day 3 after eIF6 siRNA transfection. Density gradient centrifugation of ribosomes and subsequent immunoblotting of the fractions revealed a pronounced reduction of free 60S particles in eIF6-silenced A549 cells as compared to mock transfection, suggesting a defect in 60S subunit synthesis defect (Fig. 5A*; original, non-overlayed profiles are shown in* Fig. S4A). In contrast, H520 cells showed no reduction in free 60S subunits in silenced and mock-treated cells (Fig. 5B, Fig. S3A).

Furthermore, the distribution of 40S, 60S and 80S particles in the collected fractions was analysed by immunoblotting. The small ribosomal subunit protein 3 (Rps3) served as a marker protein for the 40S and the large ribosomal subunit protein 35 (Rpl35) for the 60S subunit. WB analysis demonstrated that the majority of eIF6 sedimented in the fraction of the 60S subunit in

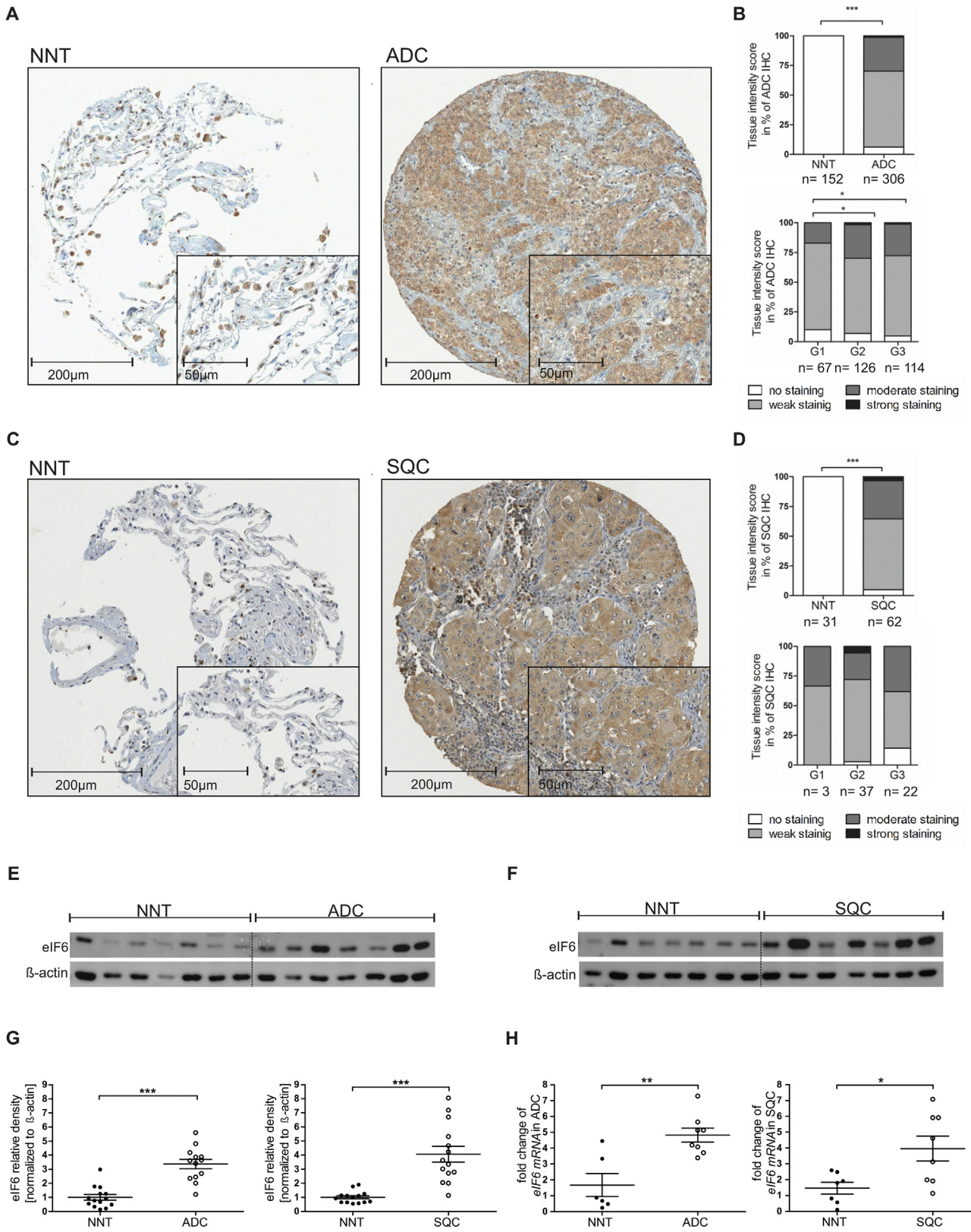

Fig. 2. eIF6 is overexpressed in NSCLC patients. **(A)** Representative IHC micrographs of eIF6-stained TMA-sections of non-neoplastic tissue (NNT) and ADC tissue. eIF6 is evident in both the nuclei and the cytoplasm of tumour cells. **(B)** Tissue intensity score analysed by Mann–Whitney U test reveals significantly stronger staining intensity of eIF6 in ADC patients as compared to NNT ($p < 0.0001$). Kruskal–Wallis test confirmed significant differences between different grades. For analysing G1 versus G2 ($p = 0.0140$) and G1 versus G3 ($p = 0.0470$) in ADC, Mann–Whitney U test was performed. **(C)** Representative IHC micrographs of eIF6-stained NNT and

Table 2
Clinicopathological characteristics of 28 patients' cryo samples.

Adenocarcinoma	n = 14	%
Gender		
Female	11	78.6
Male	3	21.4
Median age	69	
Grade		
G1	1	7.1
G2	5	35.7
G3	10	71.4
Stage[a]		
I A2	3	21.4
I B	4	28.6
II B	5	35.7
III A	2	14.3
Smoking status		
Smoker	6	42.9
Non-smoker	9	64.3
Mutation status		
EGFR	5	35.7
KRAS	5	35.7
BRAF	0	0.0
TP53	8	57.1
Squamous cell carcinoma	n = 14	%
Gender		
Female	2	14.3
Male	12	85.7
Median age	71	
Grade		
G1	2	14.3
G2	4	28.6
G3	8	57.1
Stage[a]		
I A	1	7.1
I B	4	28.6
II A	2	14.3
II B	6	42.9
III A	1	7.1
Smoking status		
Smoker	13	92.9
Non-smoker	1	7.1
Mutation status		
EGFR	0	0.0
KRAS	0	0.0
BRAF	0	0.0
TP53	11	78.6

'*Italic*' font is used for gene symbols.
[a] IASLC (International Association for the Study of Lung Cancer) 8th Edition of TNM Classification for Lung Cancer.

mock-transfected cells are associated with the 60S subunit. In the profiles of the silenced samples, eIF6 was strongly reduced, with the knockdown in the A549 cells being more efficient (Fig. 5B).

To investigate the effect of eIF6 knockdown on 60S subunit synthesis in more detail, we examined ribosomal RNA (rRNA) processing via Northern blot analysis of total RNA extracts from mock controls compared to eIF6 silenced A549 and H520 RNA extracts. We used complementary probes to the 5′-internal transcribed spacer 1 (ITS1) and internal transcribed spacer 2 (ITS2), hybridising to a range of precursor rRNA (pre-rRNA) intermediates of both ribosomal subunits. This enabled us to detect most of the major processing intermediates from both pathways. For more clarity, all known rRNA precursors are depicted in Fig. 5C, whereas the entire rRNA processing pathway is displayed in Fig. S5A. In both the cell lines, eIF6 knockdown reduced the levels of several different rRNA precursors (Fig. 5D), indicating that knockdown of eIF6 inhibits rRNA processing. The strongest effect was observed for 12S pre-rRNA, which is the precursor of the mature 5.8S rRNA component of 60S subunits. This indicates that processing of its direct precursor 32S pre-rRNA into 12S pre-rRNA and 28S pre-rRNA (not detected) is inhibited. The upstream 32S pre-rRNA was also reduced in both silenced cell lines compared to mock control. Finally, a significant decrease in 21S, 30S and 41S pre-rRNAs was observed in A549 cells after eIF6 knockdown. Considering the results of the polysome profiles, we propose that aberrant processing of the 32S pre-rRNA into its 12S downstream intermediate represents the primary defect caused by eIF6 depletion, whereas the decrease of other intermediates reflects the known feedback regulation in rRNA processing. To conclude, eIF6 knockdown leads to defective rRNA processing, resulting in reduced levels of mature 60S subunits.

4. Discussion

We present evidence that eIF6 is overexpressed in ADC and SQC compared to normal lung tissue and is a predictor for OS in ADC. Genetic interference with eIF6 by RNAi reduced cell proliferation and induced Casp 3–mediated apoptosis. In A549 cells, knockdown of

SQC tissues. eIF6 is evident in both the nuclei and the cytoplasm of tumour cells. **(D)** SQC tissue samples show a significantly higher cytoplasmic expression of eIF6 than NNT samples ($P < 0.0001$, Mann–Whitney U test). Kruskal–Wallis test did not reveal significant differences within different grades. Representative Western blots of eIF6 protein expression in ADC **(E)** and SQC **(F)** samples compared to NNT. **(G)** Densitometric analyses of eIF6 protein expression in ADC (n = 14) and SQC (n = 14) compared to NNT. The intensity of the bands was normalised to β-actin, which served as loading control. **(H)** qRT-PCR of *eIF6* mRNA was performed in 9 ADC, 9 SQC and 7 NNT samples. Fold change values of *eIF6* normalised to the mean of *ACTB and IPO8 for ADC* and for SQC *SDHA and IPO8* as housekeeping genes are depicted. *eIF6* mRNA is significantly upregulated in ADC and in SQC. Mann–Whitney U test was used for ADC data, and Student t-test was performed after ensuring Gaussian distribution on SQC data. All results shown represent mean ± SEM. (*$p < 0.05$; **$p < 0.001$; ***$p < 0.0001$). ADC, adenocarcinoma; IHC, immunohistochemistry; NSCLC, non–small cell lung cancer; SQC, squamous cell carcinoma; SEM, standard error of means; TMA, tissue microarray.

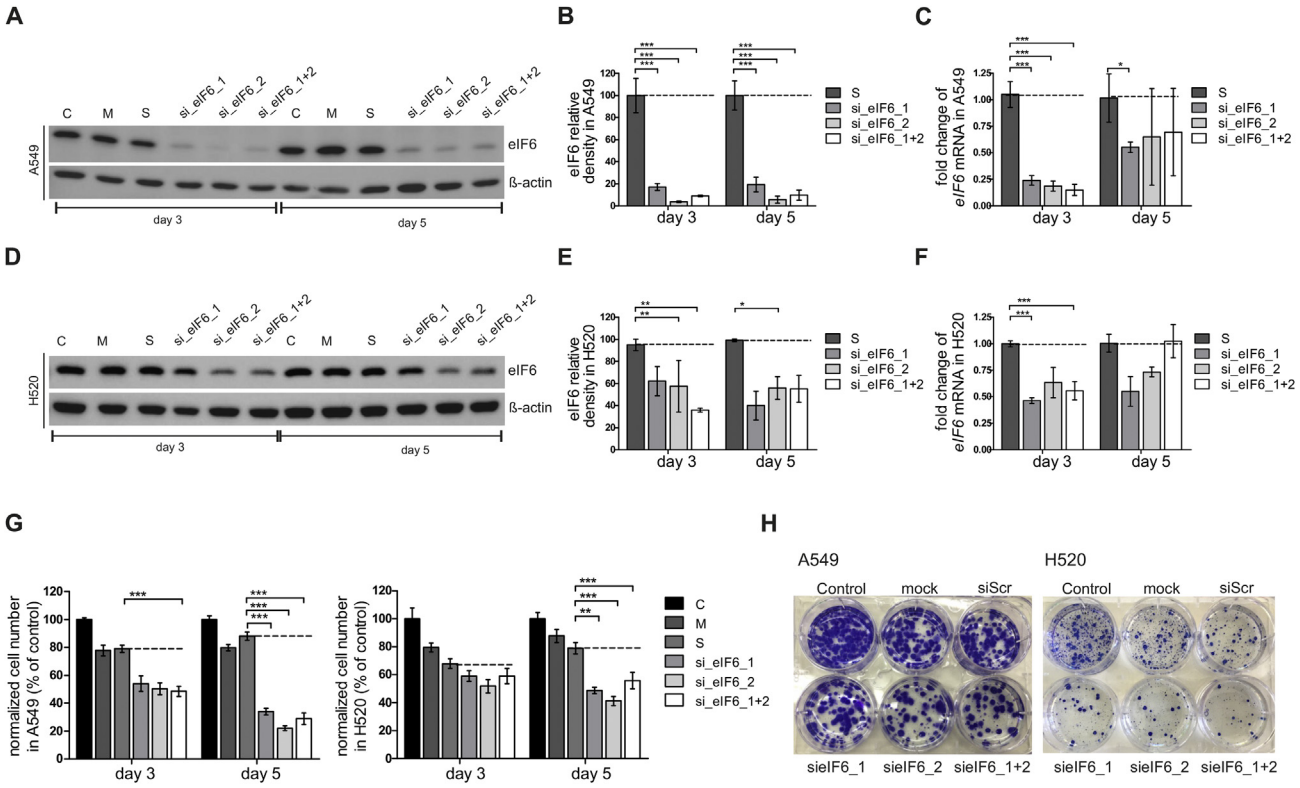

Fig. 3. Knockdown of eIF6 reduces proliferation in A549 and H520 cells. **(A)** Representative Western blots of eIF6 knockdown after 3 and 5 d in A549 cells. **(B)** Densitometric analyses of eIF6 bands normalised to β-actin, which served as loading control (one-way ANOVA). **(C)** mRNA levels of *eIF6* in transfected A549 measured by qRT-PCR and normalised to *SDHA* (one-way ANOVA). **(D)** Representative Western blots of eIF6 knockdown after 3 and 5 d in H520 cells. **E)** Densitometric analyses of eIF6 bands normalised to β-actin, which served as loading control (one-way ANOVA). **(F)** mRNA levels of *eIF6* of transfected H520 measured by qRT-PCR and normalised to *SDHA* (one-way ANOVA). **(G)** Cell numbers were counted 3 and 5 d after transfection. Data were normalised to siScr (one-way ANOVA). **(H)** Representative micrographs of colony formation of silenced A549 and H520 cells 5 d after transfection. All results shown represent mean ± SEM of three independent experiments. (*$p < 0.05$; **$p < 0.001$; ***$p < 0.0001$). ANOVA, analysis of variance; SEM, standard error of means.

eIF6 induces defects in rRNA processing, resulting in the reduction of 60S particles.

Dysregulation of eIF6 in various cancer entities, such as MPM, colorectal carcinoma (CRC), ovarian serous adenocarcinoma and head and neck cancer, was reported earlier [9,13,25,30,31]. In CRC, eIF6 is overexpressed in tumour tissue (as compared to normal mucosa) and represents a potential new therapeutic target, as well as a novel tool in surgical pathology [13,25]. Affymetrix expression data analysis performed during the present study revealed clearly that overexpression of eIF6 in lung ADC, but not in SQC, is negatively associated with patient OS. These findings were also confirmed by analysis of a second, independent TCGA data set and indicate that *eIF6* has a greater selective role on OS than eIF2alpha or eIF3B. The reason for the different impact of *eIF6* on OS in ADC and SQC is currently unclear but could, however, be associated with different mutational signatures reported for the two entities. ADCs occur primarily in the distal airways with mutations in *KRAS*, *BRAF*, *ALK*, *ROS1* and *EGFR*, whereas SQCs have mutations in *TP53* and genes of the phosphoinositide 3-kinase pathway and arise mainly in the proximal airways, presumably leading to different cellular phenotypes [3,32]. Therefore, eIF6 could fulfil different tasks in ADC and SQC.

IHC staining of ADC and SQC for eIF6 revealed overexpression in the cytoplasm of lung tumour cells but not in healthy lung tissue. For the ADC cohort analysed by TMA, we even found significant differences within increasing tumour grades. The overexpression of cytoplasmic eIF6 levels were also found in CRC, ovarian serous adenocarcinoma and MPM formalin-fixed paraffin-embedded tissue (FFPE) material [9,13,31]. Although experimentally not addressed during the present study, gene amplification could be a potential explanation for eIF6 overexpression in cancer tissue, as also discussed previously for ovarian serous carcinoma [31]. *eIF6* is located at chromosome 20 (20q12), and previous studies revealed a gain of chromosome 20

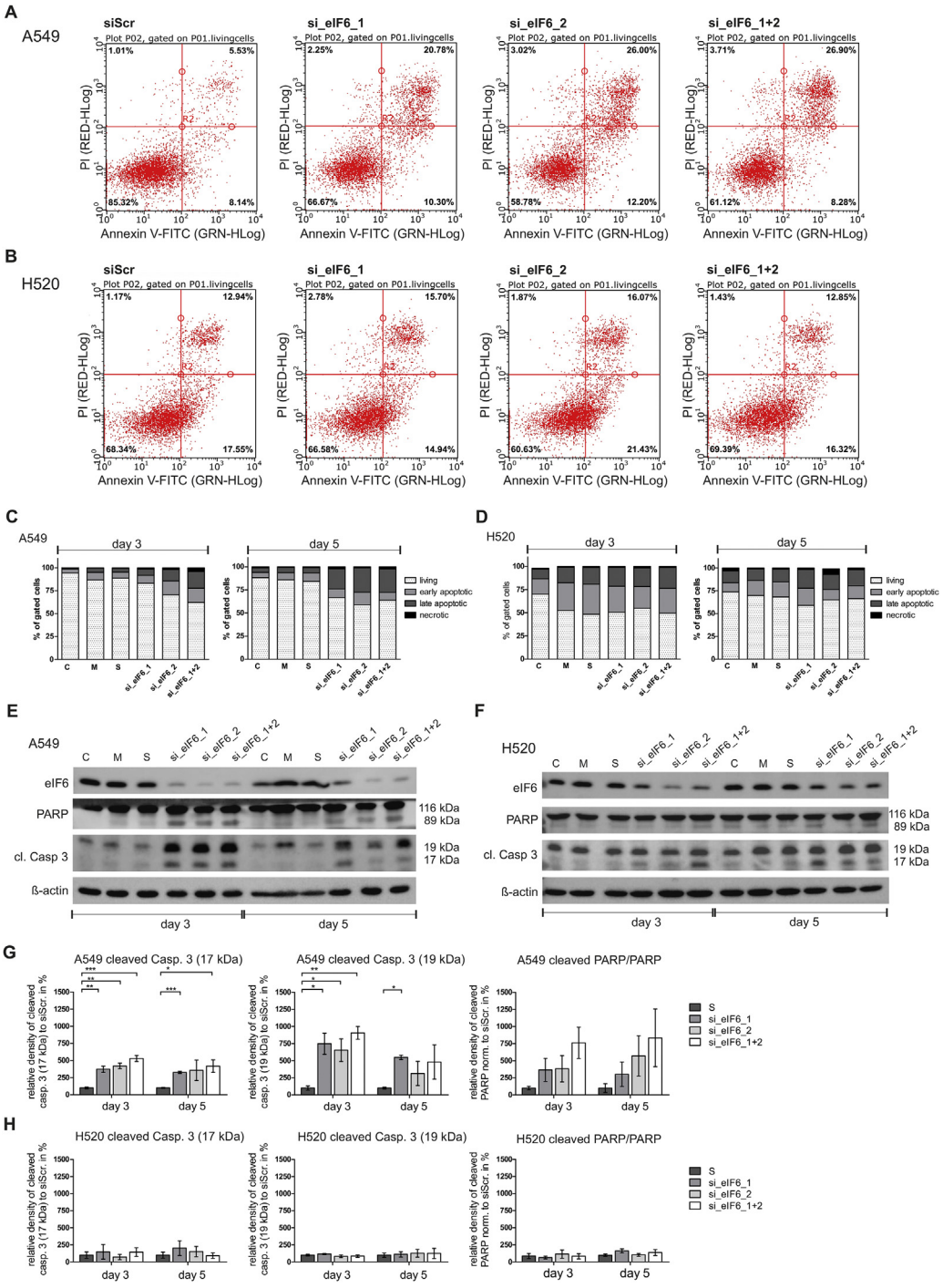

Fig. 4. Reduced eIF6 levels trigger apoptosis. Five days after transfection, **(A)** A549 and **(B)** H520 cells (siScr and siIF6 transfected) were stained with FITC Annexin V and PI and analysed by FACS. The percentage of A^-/PI^- (viable), A^+/PI^- (early apoptotic), A^-/PI^+ (late apoptotic) and A^+/PI^- (necrotic) cells is shown in **(C)** and **(D)** for A549 and H520 cells, respectively. Mean values from triplicates of two independent experiments are presented. Representative immunoblots of PARP and Casp 3 processing in response to eIF6 silencing in (**E**) A549 and (**F**) H520 cells. β-Actin served as loading control. **(G, H)** Densitometric evaluation of cleaved Casp 3 (17 kDa and 19 kDa) and cleaved PARP in **(G)** A549 and **(H)** H520 cells. Data represent mean ± SEM in three independent experiments (*$p < 0.05$; **$p < 0.001$; ***$p < 0.0001$). FACS, flow cytometric analysis; SEM, standard error of means.

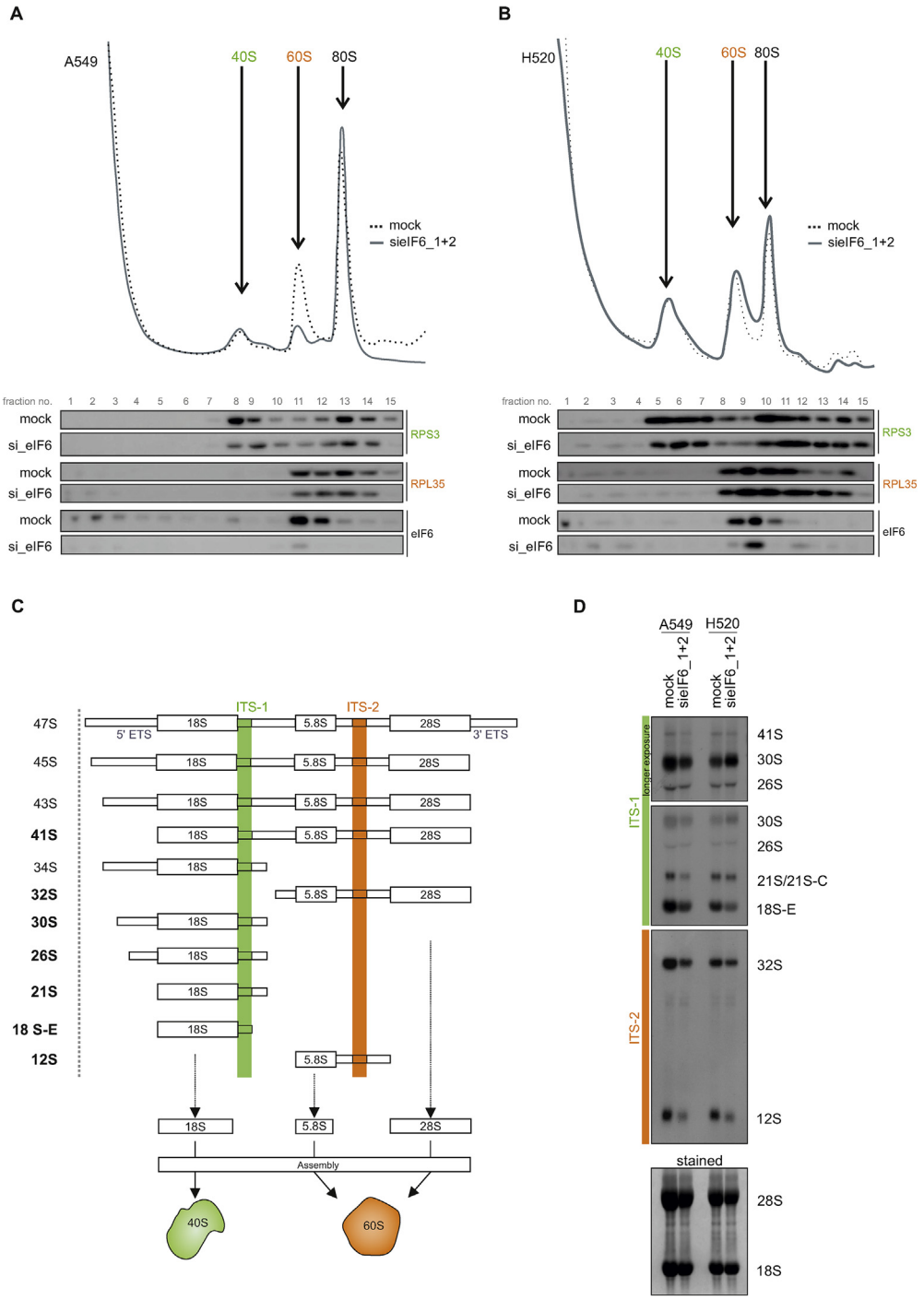

Fig. 5. rRNA processing in pre-60S subunits is disturbed by knockdown of eIF6. Sucrose density gradient profiles of transfected **(A)** A549 and **(B)** H520 cells are shown. Rpl35 antibody was used as marker for the 60S subunit and Rps3 for the 40S subunit. **(C)** Scheme of human ribosomal RNA processing, with the binding sites of the ITS1 probe, which detects 40S precursors, indicated in green, and the binding sites of the ITS2 probe detecting 60S precursors, highlighted in orange. **(D)** Representative Northern blot of eIF6-silenced A549 and H520 cells. The methylene blue–stained membrane serves as loading control and shows mature 28S and 18S ribosomal RNAs. ITS1, internal transcribed spacer 1; ITS2, internal transcribed spacer 2.

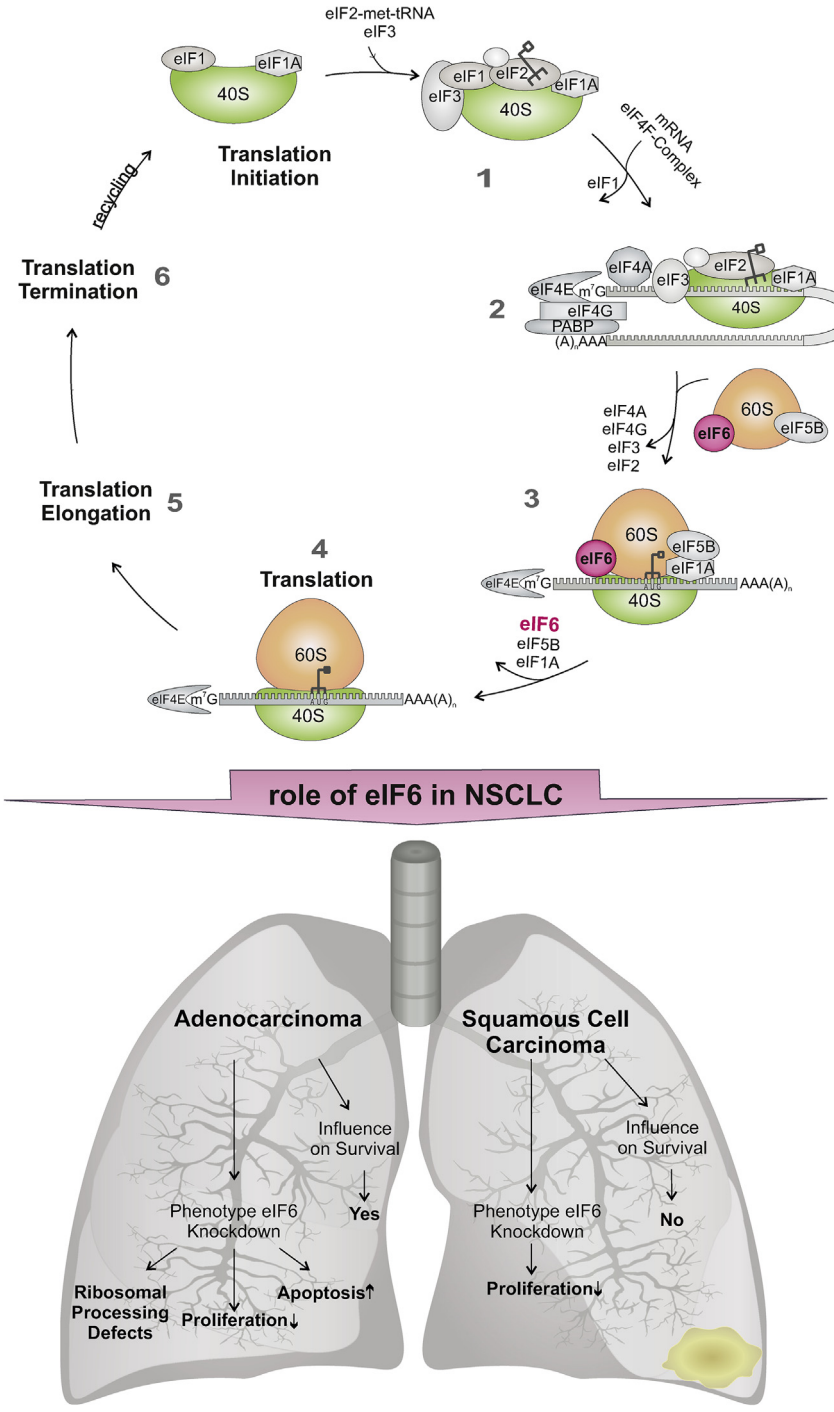

Fig. 6. Model describing the role of eIF6 in NSCLC. The eukaryotic translation initiation starts with the assembly of the 43S-initiation complex (1), in which the 40S ribosomal subunit binds to eIFs (eIF1, eIF1A, eIF3 and eIF2-met-tRNA). Subsequently, the eIF4F complex (eIF4A, eIF4G and eIF4E) accompanies the mRNA to the 43S complex and builds the pre-48S initiation complex (2). After scanning for the start codon AUG, the large ribosomal subunit 60S accompanied by eIF6 and eIF5B binds to the 48S-initiation complex (3). After the formation of a translational competent 80S ribosome, translation is initiated (4), followed by elongation (5), termination (6) and ribosomal recycling. *eIF6* is overexpressed in NSCLC and is associated with patient OS in ADC. After eIF6 knockdown in the ADC cell line decreased proliferation, increased apoptosis and ribosomal processing defects were observed. For SQC, no influence of *eIF6* on patient OS was found. The phenotype of the eIF6 knockdown in SQC cell line showed decreased proliferation. NSCLC, non–small cell lung cancer; ADC, adenocarcinoma; OS, overall survival; SQC, squamous cell carcinoma.

above ploidy level in NSCLC [33]. To unveil mechanistic details on the pathways contributing to of eIF6 overexpression in cancer tissue further experimental work is needed.

Total knockout of *eIF6* was described to be lethal in a mouse model of myc-induced lymphomagenesis in which $eIF6^{-/-}$ littermate mice were not viable. In $eIF6^{+/-}$ heterozygous knockout mice, prolonged tumour-free survival was observed, suggesting a rate-limiting role of eIF6 in tumour progression [28]. In *Saccharomyces cerevisiae*, depletion of *TIF6*, the yeast homologue of eIF6, resulted in reduced cell proliferation and viability [34].

Earlier *eIF6* knockdown studies showed that apoptosis levels were unaffected 72 h after eIF6 depletion in MPM cell line (REN cells) [9]. In the colonic carcinoma HCT116 cell line, a tendency for increased apoptosis was demonstrated after 24 h, but apoptosis was significantly reduced after 72 h [13]. In $eIF6^{+/-}$ mice, reduced eIF6 levels impaired G1/S progression in hepatic and adipose cells [35]. In contrast, proliferation in H520 cells was inhibited in response to eIF6 depletion without affecting Casp 3 or PARP processing. In the present study, we observed a clear induction of Casp 3–dependent apoptosis in A549 cells 5 d after eIF6 silencing. In A549 cells, SA-β-Gal activity and p21 levels were elevated in response to eIF6 silencing, and both parameters are indicative for the induction of cellular senescence pathways [36]. In H520 cells, no evidence for senescence could be found, and the mechanism for reduced cell growth and colony formation in this cell line is still unknown. However, it has to be considered that knockdown efficacy of eIF6 was lower in SQC cells, possibly explaining the less pronounced phenotypes. Nevertheless, the different function of eIF6 in ADC and SQC needs to be further investigated.

Ribosomal profiling revealed major 60S ribosomal subunit synthesis defects in A549 but not in H520 cells. This might be a result of lower eIF6 knockdown efficacy in SQC cells, not only for ribosomal profiles but also for pre-rRNA processing. eIF6-dependent reduction of free 60S particles was demonstrated in different experimental models (e.g. yeast, *Caenorhabditis elegans*, MPM, HeLa, ovarian carcinoma cells and mouse liver extracts) [9,24,37–39]. Pulse chase studies in yeast demonstrated that depletion of *TIF6* leads to accumulation of 27S (the analogue of human 32S) and a rapid decrease in the 7S pre-rRNA which corresponds to the human 12S precursor [34]. Northern blot analyses suggested that reduction of the 7S pre-rRNA triggers aberrant processing of downstream pre-rRNAs [34]. Data from our Northern blot analysis are reminiscent of results in the yeast system at later time points when secondary effects also evolve [34]. These data make it reasonable to assume that in the human system, eIF6 acts at a similar stage of ribosome biogenesis as Tif6 in yeast, i.e. at the conversion of the human 32S pre-rRNA (27S in yeast) into the corresponding downstream products.

5. Conclusion

We report eIF6 overexpression in NSCLC and its association with shorter patient OS in ADC. Depletion of eIF6 in lung cancer cells has an anti-tumour effect, reduces proliferation and induces apoptosis. This study provides mechanistic insights into the consequences of eIF6 depletion, revealing defects in rRNA processing. We propose eIF6 as a potential prognostic biomarker for OS in ADC. We summarised our results graphically in Fig. 6.

Author contribution

N.G., E.B., W.S. and J.H. designed and interpreted experiments. N.G. performed the experiments and wrote the manuscript. E.B., N.G.S. and S.K. interpreted biochemical analyses. N.G., I.A., L.B., H.P. and J.H. designed and interpreted histological analyses. N.G., I.A. and M.A. analysed TMA data. N.G. and C.W. conducted WB analyses. N.G. and N.G.S. performed sucrose gradient analyses. M.G.K. performed IHC. M.P. designed and evaluated the Affymetrix and TCGA analysis. H.B. and B.P. designed and interpreted the sucrose gradient analysis and edited the manuscript. V.M. performed and analysed Northern blots. N.F.N., J.L., F.G., E.S.P., L.B. and H.P. participated in recruiting and building up the study patient cohort. A.M.P. performed colony formation assay. H.P., J.H.N., J.R., A.S., C.R., C.R.D., M.N. and O.S. commented on the manuscript and interpreted data during the course of the project. J.H. devised the study and edited the manuscript, and J.H. acquired funding for conducting the entire study. All authors read and approved the final manuscript.

Conflict of interest statement

N.G., N.G.S., S.K. and J.H. hold a patent application on eIFs in NSCLC. The other authors disclose no conflicts.

Competing financial interests

Some of the authors are employees of commercial institutions: Eli Lilly (C.R.), CPO (C.R. and A.S.) and EPO (J.H. and R.J.). None of these companies have influenced the generation and interpretation of the data, neither do they profit financially from the publication of the results. The other authors declare no competing interests.

Funding

This work was carried out within K1 COMET Competence Center CBmed, which is funded by the Federal Ministry of Transport, Innovation and Technology (BMVIT); the Federal Ministry of Science, Research and Economy (BMWFW), Land Steiermark (Department 12, Business and Innovation), the Styrian Business Promotion Agency (SFG), and the Vienna Business Agency (to JH). The COMET program is executed by the FFG (no. 844609). Land Steiermark (Department 8, Science and Research) supported the publication costs (to NG). This project was carried out within the Ph.D. Program 'Molecular Medicine' at the Medical University of Graz.

Acknowledgements

The authors are grateful to Helga Reicher and Anja Feiner for their technical assistance. The authors also want to thank Anna Maria Birkl-Toeglhofer for her help with statistical analysis. The authors thank Karin Osibow for reading the manuscript.

Appendix A. Supplementary data

Supplementary data related to this article can be found at https://doi.org/10.1016/j.ejca.2018.07.001.

Appendix B. Extended methods

Patients' clinical outcome analyses

For analysing the influence of eukaryotic translation initiation factor expression on non–small cell lung cancer (NSCLC) patient clinical outcome, we used a publicly available data set generated on Affymetrix platforms as previously described (screening cohort = cohort 1) [40]. This data set contains whole transcriptome data of 1929 NSCLC patients. For data analysis, we made use of publicly available visualisation software [http://kmplot.com/analysis/index.php?p=service&cancer=lung]. Differences in OS between groups of high and low expression were tested by using a cut-off point determined automatically by the software. Survival was illustrated by Kaplan–Meier curve, and differences in survival between dichotomised groups were assessed using the log-rank test. As a second cohort (validation cohort), we analysed squamous and adenocarcinoma NSCLC cases of the Cancer Genome Atlas (TCGA) by same criteria described for cohort 1.

Tissue microarray (TMA) generation and evaluation

TMAs were constructed at the Diagnostic and Research Institute of Pathology, Medical University of Graz, Austria. Formalin-fixed paraffin-embedded samples of lung carcinoma from a total of 414 patients were collected and used for the generation of 5 TMAs (4 ADCs and 1 SQC). Haematoxylin-eosin–stained slides of specimens were reviewed by three experienced, board-certified pathologists (H.P., L.B. and J.H.). The use of patient samples for the TMAs was approved by the local Ethics Committee (No. 24-135 ex 11/12). The pattern of IHC staining was evaluated by four independent examiners (J.H., I.A., L.B. and NG) by light microscopy. Each core was semi-quantitatively scored, and an intensity score was assessed as follows: 0 = no staining, 1 = weak staining, 2 = moderate staining and 3 = strong staining. In addition, a percentage of stained tumour cells was recorded (0–100%) and grouped into five groups: 0 = 0%, 1 = 1–≤10%, 2 = 11–49%, 3 = 50–79% and 4 = ≥80%. Intensity score (0–3) was then multiplied by percentage score (0–4), and obtained values were grouped as follows: 0 = no staining, 1–4 = weak staining, 4–8 = moderate staining and 8–12 = strong staining and displayed in stacked plots.

Immunohistochemistry

Immunohistochemistry (IHC) was performed on 3-μm-thick sections of each TMA. Primary eIF6 antibody (clone A303-030A, Bethyl, Montgomery, USA) was stained on a Ventana Immunostainer XT with Ultra View DAB detection Kit and CC1 as epitope retrieval. Counterstaining with Haematoxylin followed.

Human lung cancer patient samples

Human lung cancer samples and non-neoplastic lung tissues (NNT) were obtained at the Diagnostic and Research Institute of Pathology, Medical University of Graz, Graz, Austria. Informed consent forms from the patients were obtained. Samples were collected during frozen section and immediately flash frozen in liquid nitrogen and stored until protein or RNA was extracted.

Protein extraction and WB analysis

For generation of protein lysates, frozen lung ADC and SQC tissue samples were homogenised using a MagNa Lyser homogeniser (Roche Diagnostics, Risch-Rotkreuz, Switzerland) in lysis buffer (0.05 M Tris-HCl, 0.15 M NaCl, 0.5% NP-40, 0.1 M Pefabloc, 1 mM dithiothreitol [DTT], complete Mini, PhosSTOP). Phosphate-buffered saline (PBS)–washed A549 and H520 cells were scraped in lysis buffer. Protein concentrations were determined using Bradford protein assay (Biorad Protein Assay Dye Reagent, 500-0006; Biorad Protein Laboratories Inc. Germany). Twenty micrograms of protein lysates was loaded on 12.5% sodium dodecyl sulfate polyacrylamide gel electrophoresis (SDS-PAGE). Western blotting was

performed as previously described [13]. Membranes were probed with primary antibodies listed in Table S1 in Tris-buffered saline with Tween20 (TBST), 5% bovine serum albumin overnight at 4 °C, followed by incubation with the secondary antibody. ImageQuant LAS 500 (GE Health Care, Little Chalfont, UK) was used as the detection system.

RNA isolation for real-time-PCR and Northern blots

Total RNA was isolated from human snap frozen ADC, SQC and NNT lung tissue, as well as from A549 and H520 cells. RNA was extracted via phenol–chloroform extraction. Cells were lysed in Trizol® Reagent (Thermo Fischer Scientific Inc., Massachusetts, USA) before the addition of chloroform. After centrifugation, the aqueous phase was precipitated with isopropanol. The pellet was washed twice with 80% alcohol and dissolved in RNase-free water. RNA concentration in the supernatant was determined via Nanodrop1000 (Thermo Fischer scientific, Massachusetts, USA).

Quantitative real-time-PCR

100 nanograms RNA was reversely transcribed with High-Capacity cDNA Reverse Transcription Kit (Applied Biosystems, Foster City, USA) according to the manufacturer's instructions using the GeneAmp 9700 Thermocycler (Applied Biosystems; Foster City, USA). qRT-PCR was performed using SYBR Green PCR Master Mix Kit (Applied Biosystems, Foster City, USA) and Quant Studio 7 Flex (Applied Biosystems; Foster City, USA). The most stable housekeeping genes (HKG) were determined based on the algorithm implemented in NormFinder Software [41]. For ADC tissue samples, succinate dehydrogenase complex, subunit A (*SDHA*) and Importin 8 (*IPO8*) and for SQC tissue samples, *β-actin* and *SDHA* were calculated to be most stable HKGs. Fold change values of *eIF6* were normalised to the mean ct-values of HKGs. For cell culture (A549, H520) experiments, *β-actin* served as internal control. Primer sequences are shown in Suppl. Table S2. Fold change levels were analysed using the $2^{-\Delta\Delta}$CT method [42].

Cell cultures

The human lung adenocarcinoma cell line A549 (cat. no. 300114) was purchased from CLS Cell Lines Service GmbH (Eppelheim, Germany) and cultured in Dulbecco's Modified Eagle Medium (DMEM): Hams-F12 (no. 11330-57, Life Technologies, California, USA) supplemented with 10% fetal bovine serum (FBS) (no. 10270-106, Gibco, Life Technologies, California, USA) and 1% penicillin/streptomycin (Gibco, Life Technologies, California, USA). The human squamous cell carcinoma cell line H520 was obtained from ATCC (NCI-H520) and cultured in DMEM supplemented with 10% FBS and 1% penicillin/streptomycin. For cell detachment, either Trypsin plus ethylene diamine tetra-acetic acid (EDTA) 0.05% (Life Technologies, California, USA) for A549 cells or Accutase® solution (Sigma Aldrich, Missouri, USA) for H520 cells was used. Both the cell lines were incubated at 37 °C in a humidified atmosphere containing 5% CO_2. All cells were tested every 3–6 months for mycoplasma contamination using PromoKine PCR Mycoplasma (Biomedica Medizinprodukte GmbH & Co KG, Vienna, Austria).

siRNA transfection

Cell cycle was synchronised by serum starvation for 16 h before seeding of 2×10^4 cells/well of A549 and 8×10^4 cells/well of H520 on 12 well plates. Transfection was performed with Oligofectamine™ Transfection Reagent (Life Technologies, California, USA) according to the manufacturer's instructions. The siRNA oligonucleotides are listed in Table S3.

Proliferation assay

Cells were seeded into 12-well culture plates and transfected with specific siRNA (20 nM) after 24 h. At day 3 and 5 after transfection, cells were trypsinised, and the cell number was determined by Guava ViaCount Assay (Millipore, Massachusetts, USA) on Guava EasyCyte 8 (Millipore, Massachusetts, USA).

Annexin V/propidium iodide staining

For annexin V/propidium iodide (PI) staining, A549 and H520 cells were transfected with 20 nM of eIF6-specific or non-targeting siRNAs. Three and 5 d after transfection cells, supernatants were harvested and stained using the FITC Annexin V Apoptosis Detection Kit (#640932, Biolegend, San Diego, CA, USA) according to the manufacturer's suggestion. Supernatants were collected before detachment of adherent cells by either trypsin or accutase for A549 and H520, respectively. Subsequently, cells were washed with cold PBS and incubated with 100 µl of 1× binding buffer (containing 5 µl of Annexin V FITC and 5 µl of PI) for 15 min (25 °C) in the dark [43,44]. FACS was performed using Guava EasyCyte 8 (Millipore, Billerica, MA, USA) and analysed with InCyte 3.1 (Millipore). To set up fluorescence compensation and gating for detection of necrosis and early/late apoptosis, unstained and single-stained cells were treated with staurosporine (1 µM, 4 h, Sigma Aldrich, Missouri, USA).

Senescence analysis

For detection of senescence-associated β-galactosidase (SA-β-Gal) activity, we followed the protocol described

by Dimri *et al.* [45]. The assay was performed on day 4 after transfection. Untreated, mock and siScr-transfected cells were used as controls. Experiments were performed in triplicate.

Colony formation assay

After inducible knockdown of eIF6 in A549 or H520, 400 cells were collected after 3 d and seeded in 6-well plates. After 4 weeks, cells were fixed with 4% paraformaldehyde (Sigma–Aldrich, Missouri, USA), stained with Giemsa solution (Sigma–Aldrich, Missouri, USA) for 20 min and rinsed with distilled water.

Sucrose gradient fractionation and ribosome-associated protein analysis

Sucrose density gradient centrifugation separates polysomes, 80S ribosomes and free 40S and 60S ribosomal subunits. A549 and H520 cells were cultured for 3 d in 100-mm dishes and transfected with siRNA (eIF6_1 + 2), with mock as a control. Fifteen minutes before lysis, cells were incubated with 100 μg/ml cycloheximide (CHX) (Sigma–Aldrich, Missouri, USA) to inhibit translation. Before scraping in lysis buffer (20 mM 4-(2-hydroxyethyl)-1-piperazineethanesulfonic acid (HEPES) pH 7.4, 15 mM $MgCl_2$, 200 mM KCl, 1% Triton X-100, 2 mM DTT and 100 μg/ml cycloheximide), cells where washed with ice-cold PBS containing 100 μg/ml CHX. After centrifugation (14,000g, 10 min, 4 °C), RNA concentration in the supernatant was determined via Nanodrop1000 (Thermo Fischer Scientific Inc., Massachusetts, USA). Three OD_{260} units were layered onto 15–40% sucrose gradients (50 mM NH_4Cl, 50 mM Tris-acetate pH 7.0, 12 mM $MgCl_2$, freshly added 100 μg/ml cycloheximide and 1 mM DTT) and centrifuged in a SW41Ti rotor (Beckman, Villepinte, France) for 150 min at 160,000g, 4 °C without breaking. Ribosomal profiles were recorded via an ISCO (Teledyne ISCO, Nebraska, USA) density gradient–analysing unit, which includes a UA-6 detector that measures the absorption at 254 nm, allowing for detection of RNA. As the majority of cellular RNAs are contained in ribosomes, this analysis records the ribosomal distribution.

Fractions were collected along the gradients and precipitated with trichloroacetic acid overnight at −20 °C to concentrate proteins for gel electrophoresis and subsequent WB analysis.

Northern blotting

Five micrograms of RNA per sample was separated on 1.5% 3-(N-morpholino)propanesulfonic acid (MOPS)-agarose gels as described in the manual of the RNeasy minikit (QIAGEN, Hilden, Germany). The RNA was transferred overnight onto a Hybond N nylon membrane (GE Health Care, Little Chalfont, UK) and then cross-linked to the membrane by UV light. Membranes were stained with 0.02% methylene blue and 3% acetic acid to visualise the mature 28S and 18S rRNAs. Hybridisation was performed overnight at 37 °C in 500 mM NaH_2PO_4 buffer, pH adjusted to 7.2 with H_3PO_4, 7% SDS, 1 mM EDTA using 5′-^{32P}-labelled oligonucleotides with the following sequences: ITS1, 5′-CCTCGCCCTCCGG GCTCCGTTAATGATC-3′; ITS2, 5′-CTGCGAGG-GAACCCCCAGCCGCGCA-3′. The membranes were washed three times for 20 min at 37 °C in 40 mM NaH_2PO_4 buffer, pH was adjusted to 7.2 with H_3PO_4, 1% SDS, and radioactivity was detected by exposing to X-ray films. Membranes were regenerated by washing in 1% SDS.

References

[1] Siegel RL, Miller KD, Jemal A. Cancer statistics, 2016. CA Cancer J Clin 2016;66:7–30. https://doi.org/10.3322/caac.21332.

[2] Howlader N, Noone A, Krapcho M, Miller D, Bishop K, Kosary C, et al. SEER cancer statistics review, 1975-2014. Bethesda, MD: Natl Cancer Institute; 2017.

[3] Chen Z, Fillmore CM, Hammerman PS, Kim CF, Wong K-K. Non-small-cell lung cancers: a heterogeneous set of diseases. Nat Rev Cancer 2014;14:535–46. https://doi.org/10.1038/nrc3775.

[4] Davidson MR, Gazdar AF, Clarke BE. The pivotal role of pathology in the management of lung cancer. J Thorac Dis 2013;5(Suppl. 5): S463–78. https://doi.org/10.3978/j.issn.2072-1439.2013.08.43.

[5] Meric-Bernstam F, Hunt KK. Translation initiation in cancer: a novel target for therapy. Mol Cancer Ther 2002;1:971–9.

[6] Spilka R, Ernst C, Bergler H, Rainer J, Flechsig S, Vogetseder A, et al. eIF3a is over-expressed in urinary bladder cancer and influences its phenotype independent of translation initiation. Cell Oncol 2014;37:253–67. https://doi.org/10.1007/s13402-014-0181-9.

[7] Xu G, Yu H, Shi X, Sun L, Zhou Q, Zheng D, et al. Cisplatin sensitivity is enhanced in non-small cell lung cancer cells by regulating epithelial-mesenchymal transition through inhibition of eukaryotic translation initiation factor 5A2. BMC Pulm Med 2014;14:174. https://doi.org/10.1186/1471-2466-14-174.

[8] Demosthenous C, Han JJ, Stenson MJ, Maurer MJ, Wellik LE, Link B, et al. Translation initiation complex eIF4F is a therapeutic target for dual mTOR kinase inhibitors in non-Hodgkin lymphoma. Oncotarget 2015;6:9488–501. https://doi.org/10.18632/oncotarget.3378.

[9] Miluzio A, Oliveto S, Pesce E, Mutti L, Murer B, Grosso S, et al. Expression and activity of eIF6 trigger malignant pleural mesothelioma growth in vivo. Oncotarget 2015;6:37471–85. https://doi.org/10.18632/oncotarget.5462.

[10] Vaysse C, Philippe C, Martineau Y, Quelen C, Hieblot C, Renaud C, et al. Key contribution of eIF4H-mediated translational control in tumor promotion. Oncotarget 2015;6:39924–40. https://doi.org/10.18632/oncotarget.5442.

[11] Dai L, Lin Z, Cao Y, Chen Y, Xu Z, Qin Z. Targeting EIF4F complex in non–small cell lung cancer cells. Oncotarget 2017;8:1–5.

[12] Golob-Schwarzl N, Krassnig S, Toeglhofer AM, Park YN, Gogg-Kamerer M, Vierlinger K, et al. New liver cancer biomarkers: PI3K/AKT/mTOR pathway members and eukaryotic translation initiation factors. Eur J Cancer 2017;83:56–70. https://doi.org/10.1016/j.ejca.2017.06.003.

[13] Golob-Schwarzl N, Schweiger C, Koller C, Krassnig S, Gogg-Kamerer M, Gantenbein N, et al. Separation of low and high

grade colon and rectum carcinoma by eukaryotic translation initiation factors 1, 5 and 6. Oncotarget 2017;8:101224–43. https://doi.org/10.18632/oncotarget.20642.
[14] Silvera D, Formenti SC, Schneider RJ. Translational control in cancer. Nat Rev Cancer 2010;10:254–66. https://doi.org/10.1038/nrc2824.
[15] Sonenberg N, Hinnebusch AG. Regulation of translation initiation in eukaryotes: mechanisms and biological targets. Cell 2009;136:731–45. https://doi.org/10.1016/j.cell.2009.01.042.
[16] Jackson RJ, Hellen CUT, Pestova TV. The mechanism of eukaryotic translation initiation and principles of its regulation. Nat Rev Mol Cell Biol 2010;11:113–27. https://doi.org/10.1038/nrm2838.
[17] Klinge S, Voigts-Hoffmann F, Leibundgut M, Arpagaus S, Ban N. Crystal structure of the eukaryotic 60S ribosomal subunit in complex with initiation factor 6. Science (80-) 2011;334:941–8. https://doi.org/10.1126/science.1211204.
[18] Khatter H, Myasnikov AG, Natchiar SK, Klaholz BP. Structure of the human 80S ribosome. Nature 2015;520:640–5. https://doi.org/10.1038/nature14427.
[19] Brina D, Miluzio A, Ricciardi S, Biffo S. eIF6 anti-association activity is required for ribosome biogenesis, translational control and tumor progression. Biochim Biophys Acta - Gene Regul Mech 2015;1849:830–5. https://doi.org/10.1016/j.bbagrm.2014.09.010.
[20] Weis F, Giudice E, Churcher M, Jin L, Hilcenko C, Wong CC, et al. Mechanism of eIF6 release from the nascent 60S ribosomal subunit. Nat Struct Mol Biol 2015;22. https://doi.org/10.1038/nsmb.3112.
[21] Tafforeau L, Zorbas C, Langhendries J-L, Mullineux S-T, Stamatopoulou V, Mullier R, et al. The complexity of human ribosome biogenesis revealed by systematic nucleolar screening of Pre-rRNA processing factors. Mol Cell 2013;51:539–51. https://doi.org/10.1016/j.molcel.2013.08.011.
[22] Lafontaine DLJ. Noncoding RNAs in eukaryotic ribosome biogenesis and function. Nat Struct Mol Biol 2015;22:11–9. https://doi.org/10.1038/nsmb.2939.
[23] Valenzuelas DM, Chaudhurig A, Maitra U. Eukaryotic ribosomal aubunit anti-association activity of calf liver Is contained in a single polypeptide chain protein of MI. = 25,500 (eukaryotic initiation factor 6). J Biol Chem 1982;257:7712–9.
[24] Ceci M, Gaviraghi C, Gorrini C, Sala LA, Offenhäuser N, Marchisio PC, et al. Release of eIF6 (p27BBP) from the 60S subunit allows 80S ribosome assembly. Nature 2003;426:579–84. https://doi.org/10.1038/nature02160.
[25] Sanvito F, Vivoli F, Gambini S, Santambrogio G, Catena M, Viale E, et al. Expression of a highly conserved protein, p27 BBP, during the progression of human colorectal cancer. Cancer Res 2000;60:510–6.
[26] Brina D, Grosso S, Miluzio A, Biffo S. Translational control by 80S formation and 60S availability: the central role of eIF6, a rate limiting factor in cell cycle progression and tumorigenesis. Cell Cycle 2011;10:3441–6. https://doi.org/10.4161/cc.10.20.17796.
[27] Pinzaglia M, Montaldo C, Polinari D, Simone M, La Teana A, Tripodi M, et al. EIF6 over-expression increases the motility and invasiveness of cancer cells by modulating the expression of a critical subset of membrane-bound proteins. BMC Cancer 2015;15:131. https://doi.org/10.1186/s12885-015-1106-3.
[28] Miluzio A, Beugnet A, Grosso S, Brina D, Mancino M, Campaner S, et al. Impairment of cytoplasmic eIF6 activity restricts lymphomagenesis and tumor progression without affecting normal growth. Cancer Cell 2011;19:765–75. https://doi.org/10.1016/j.ccr.2011.04.018.
[29] Gatza ML, Silva GO, Parker JS, Fan C, Perou CM. An integrated genomics approach identifies drivers of proliferation in luminal-subtype human breast cancer. Nat Genet 2014;46:1051–9. https://doi.org/10.1038/ng.3073.
[30] Rosso P, Cortesina G, Sanvito F, Donadini A, Di Benedetto B, Biffo S, et al. Overexpression of p27BBP in head and neck carcinomas and their lymph node metastases. Head Neck 2004;26:408–17. https://doi.org/10.1002/hed.10401.
[31] Flavin RJ, Smyth PC, Finn SP, Laios A, O'Toole SA, Barrett C, et al. Altered eIF6 and dicer expression is associated with clinicopathological features in ovarian serous carcinoma patients. Mod Pathol 2008;21:676–84. https://doi.org/10.1038/modpathol.2008.33.
[32] Kenfield SA, Wei EK, Stampfer MJ, Rosner BA, Colditz GA. Comparison of aspects of smoking among four histologic types of lung cancer. Tob Control 2011;17:198–204. https://doi.org/10.1136/tc.2007.022582.Comparison.
[33] Berrieman HK, Ashman JNE, Cowen ME, Greenman J, Lind MJ, Cawkwell L. Chromosomal analysis of non-small-cell lung cancer by multicolour fluorescent in situ hybridisation. Br J Cancer 2004;90:900–5. https://doi.org/10.1038/sj.bjc.6601569.
[34] Basu U, Si K, Warner JR, Maitra U. The *Saccharomyces cerevisiae* TIF6 gene encoding translation initiation factor 6 is required for 60S ribosomal subunit biogenesis. Society 2001;75:1453–62. https://doi.org/10.1128/MCB.21.5.1453.
[35] Gandin V, Miluzio A, Barbieri AM, Beugnet A, Kiyokawa H, Marchisio PC, et al. Eukaryotic initiation factor 6 is rate-limiting in translation, growth and transformation. Nature 2008;455:684–8. https://doi.org/10.1038/nature07267.
[36] Bernhart E, Damm S, Heffeter P, Wintersperger A, Asslaber M, Frank S, et al. Silencing of protein kinase D2 induces glioma cell senescence via p53-dependent and -independent pathways. Neuro Oncol 2014;16:933–45. https://doi.org/10.1093/neuonc/not303.
[37] Chendrimada TP, Finn KJ, Ji X, Baillat D, Gregory RI, Liebhaber SA, et al. MicroRNA silencing through RISC recruitment of eIF6. Nature 2007;447:823–8. https://doi.org/10.1038/nature05841.
[38] Benelli D, Cialfi S, Pinzaglia M, Talora C, Londei P. The translation factor eIF6 is a notch-dependent regulator of cell migration and invasion. PLoS One 2012;7:e32047. https://doi.org/10.1371/journal.pone.0032047.
[39] Finch AJ, Hilcenko C, Basse N, Drynan LF, Goyenechea B, Menne TF, et al. Uncoupling of GTP hydrolysis from eIF6 release on the ribosome causes Shwachman-Diamond syndrome. Genes Dev 2011;25:917–29. https://doi.org/10.1101/gad.623011.
[40] Győrffy B, Surowiak P, Budczies J, Lánczky A. Online survival analysis software to assess the prognostic value of biomarkers using transcriptomic data in non-small-cell lung cancer. PLoS One 2013;8:e82241. https://doi.org/10.1371/journal.pone.0082241.
[41] Andersen CL, Jensen JL, Ørntoft TF. Normalization of real-time quantitative reverse transcription-PCR data: a model-based variance estimation approach to identify genes suited for normalization, applied to bladder and colon cancer data sets. Cancer Res 2004;64:5245–50. https://doi.org/10.1158/0008-5472.CAN-04-0496.
[42] Livak KJ, Schmittgen TD. Analysis of relative gene expression data using real-time quantitative PCR and the 2−ΔΔCT method. Methods 2001;25:402–8. https://doi.org/10.1006/meth.2001.1262.
[43] Liu Y, Sturgis CD, Grzybicki DM, Jasnosz KM, Olson PR, Tong M, et al. Microtubule-associated protein-2: a new sensitive and specific marker for pulmonary carcinoid tumor and small cell carcinoma. Mod Pathol 2001;14:880–5. https://doi.org/10.1038/modpathol.3880406.
[44] Olsen BB, Wang S-Y, Svenstrup TH, Chen BP, Guerra B. Protein kinase CK2 localizes to sites of DNA double-strand break regulating the cellular response to DNA damage. BMC Mol Biol 2012;13:7. https://doi.org/10.1186/1471-2199-13-7.
[45] Dimri GP, Lee X, Basile G, Acosta M, Scott G, Roskelley C, et al. A biomarker that identifies senescent human cells in culture and in aging skin in vivo. Proc Natl Acad Sci USA 1995;92:9363–7.